Bias Choke

Maryse Ernzer
Semesterthesis, Departement Physik, ETH Zürich

December 14, 2016

Abstract

The bias choke is mainly bulit up of a single layer toroid iron core inductor used to add two different inputs, namely a DC bias and a high frequency pulse. The essential feature of the final design consists in a low cutoff frequency of the inductor, a flat tranmission with low attenuation above the cutoff frequency, as well as a good temperature stablility for the device to work at very low temperatures . All of this properties are important to bias the high frequency pulse without distorting it. The challenge consists in correctly modeling the behavior of the inductor as a transmission line in order to remove all resonance effects from the considered frequency range.

Contents

1 Introduction

The design of the bias choke aims to apply a DC current to the flux lines instead of using coils to tune the frequency of the qubits, because of the limited space on the sample holder underneath the qubit chip. Figure 1 shows the insertion of the bias choke into the final experimental setup.

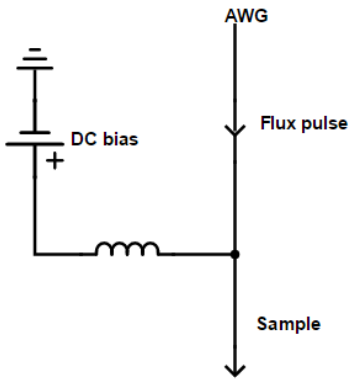

Figure 1: Circuit diagram of the placement of the bias choke in the final experimental setup

On the one hand the bias choke has to be very stable and predictable in its transmission and show little attenuation to precisley tune the qubits. That's why the resonance features, which would allow certain frequencies to pass through the inductor, have to be removed from the considered frequency range. Also the cutoff frequency has to be very low in order for the inductor to function as an ideal low pass filter and to maintain the whole microwave pulse on the through line, preventing it from leaving through the dc line.

On the other hand the bias choke needs to show a steady performance under low temperartures as it will be installed on a 20mK plate. Furthermore the heat production has to be minimzed, considering the limited cooling power available at these temperatures.

2 Theory on inductors

Measuring the scattering parameters of an inductor one notices resonance peaks, meaning above the self-resonance frequency one sees dips in the transmission which are due to variations in the inductance of the coil. These changes are caused by the reactance of a coil looking like an inductance in parallel with a parasitic capacitance, which makes the inductor an effective LC circuit shown in Figure 2 and generates a self-resonance at $f_r = 1/2\pi\sqrt{LC}$ (SRF). The parasitic capacitances are often explained by the adjacent single windings which are parallel wires functioning as capacitors. This model suggests to use an inductor with a high permeability and as few

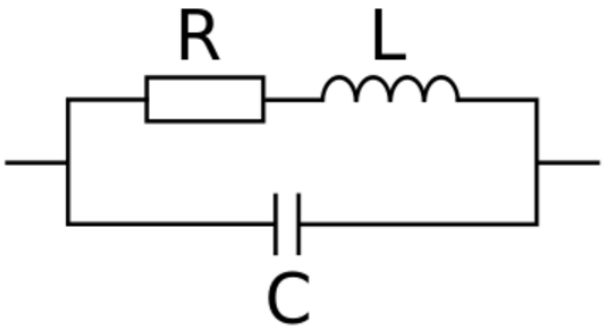

Figure 2: Schematic equivalent circuit of a real inductor, with L the effective inductance, C the parasitic capacitance and R the resistane of the windings [7]

windings as possible to minimize the resonance effects. In fact the lumped element predictions are in good agreement with what one sees up to the SRF, but gives no explanation for the additional resonances at higher frequencies besides the fundamental SRF. However for higher frequencies where one can no longer consider an electrical circuit as built from lumped elements, the windings around the coil have to be regarded as a transmission line and the resonances in the inductance as standing waves due to the difference in the magnetic environment leading to impedance discontinuities as the wire gets around the coil.

The standing waves produce resonances at wavelengths which are even multiples of the path length so that the self-resoance frequency is given by $f_r = \frac{c}{2l_{path}\sqrt{\mu}}$ Hz with $l_{path} = \sqrt{(Nl_p)^2 + (\alpha l_e)^2}$, l_p the length of the periphery of the toroids cross-section, l_e the length of the magnetic path, α the fraction of the toroid circumference covered by the winding. [5] Using this expression for the SRF which depends only on the dimensions of the coil and the number of windings we can compute the self-capacitance of the coil, as well as the apparent inductance,

$$C_{self} = -\frac{1}{(2\pi f_r)^2 L_0} \tag{1}$$

with $L_0 = A_L N^2$ the inductance at low frequencies, (for further explanations of the inductance factor A_L see next section).

$$L_{app} = -\frac{X_L X_C}{\omega(X_L - X_C)} \tag{2}$$

where $X_L = \omega L_0$ and $X_C = \frac{1}{\omega C_{self}}$

Additional to the parasitic inter-winding capacitance there is also a gap capacitance, a true capacitance between the emerging wires. For the type of coils we use it is about the order of 0.5 pF. That's why the distance between the in and out going wire as well as between the adjacent windings should be maximized. This leads to an optimal opening angle between the in and out going wires of 30° an evenly spread windings.

3 Experimental setup

As we want to design the bias choke as small as possible we are using T-37 iron powder toroids which have an outer diameter of 9.53 mm and a height of 3.25 mm. Looking for a compromise between a good temperature stability and a high permeability we choose the iron powder core material 2 with A_L=40 μH/100 turns and temperature stability 95 ppm/°C as well as material 3 with A_L=120 μH/100 turns and temperature stability 370 ppm/°C. Noting that in this case the units of the inductance factor A_L are given as inductance per hundred turns, whereas it is often expressed in inductance per turn squared such that L=$A_L N^2$. Figure 3 shows such a toroidal coil material 3 wrapped with 15 windings of an enameled copper wire.

Figure 3

In order to analyze the scattering parameters of the coil with a VNA we put it in a SMA connector box. To simulate the final use of the coil placed on the dc line we solder two SMP connectors together which we can place on the through line of the VNA and use the third pin to solder the coil to.

Later on we are also going to test three different SMD inductors, namely the semi-shielded power inductor 300-26-154 with an inductance of 0.47 μH, a self-resonance frequency around 230 MHz,composed of an epoxy-ferrite powder mixture resin enveloping the tightly coiled conductive wire which makes it of a minitiare size of $2 \times 1.6 \times 1$ mm. [6]. Then we are also going to use the very similar inductor 300-41-940 which has an inductance of 0.47 μH, but which is of a slightly bigger size, has a self-resonance frequency around 304 MHz and a magnetic resin used for the magnetic shielding. Last we are going to test the magnetically shielded 300-42-407 SMD inductor which has an inductance of 0.68μH, a self-resonance frequency of 265MHz and a flat wire coil for low losses at high frequency.

4 Measurements

4.1 Toroidal inductors

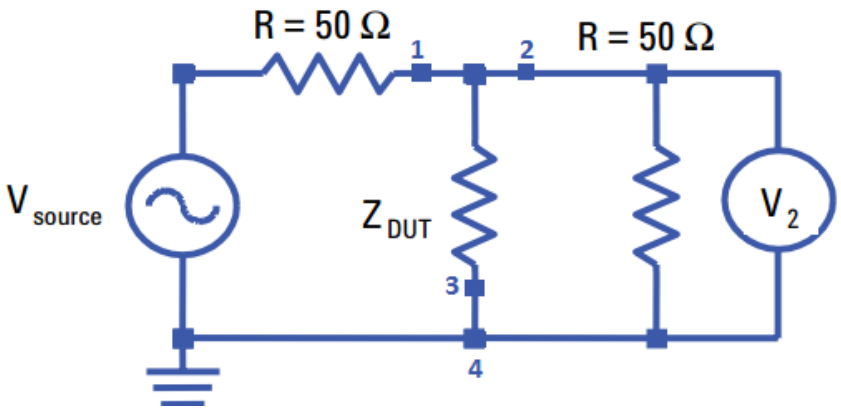

Figure 4: Schematic quivalent circuit of VNA measurement with Z_{DUT} the device under test [4]

First the two SMP connectors are soldered together, shown in Figure 5 using a solder paste and put on the through line, meaning between points 2 and 3 in Figure 4 of the VNA. Subsequently it is measured over frequency range from 300 kHz to 1.0 GHz. One can see from Figure 6 that the transmission shows nearly no attenuation so that it is suitable to join the coil to the high frequency line in the following measurements.

Figure 5

To see the behavior of the coil 2 with 15 windings separatley, we put it inside a SMA connector box, insert it between points 1 and 2 and take a measurement over a frequency range from 0.03-1.0 GHz. From Figure 7 we can see a difference between the case where the box is closed compared to the open case, which is due to resonances within the box. However in both cases we can observe a dip in the transmission around 0.3 GHz which corresponds to the self-resonance frequency of the coil. The theoretical prediction has been computed using formulas 3 and 2 and inverting to get an expression for S_{21}.

In order to compare our measurement to the

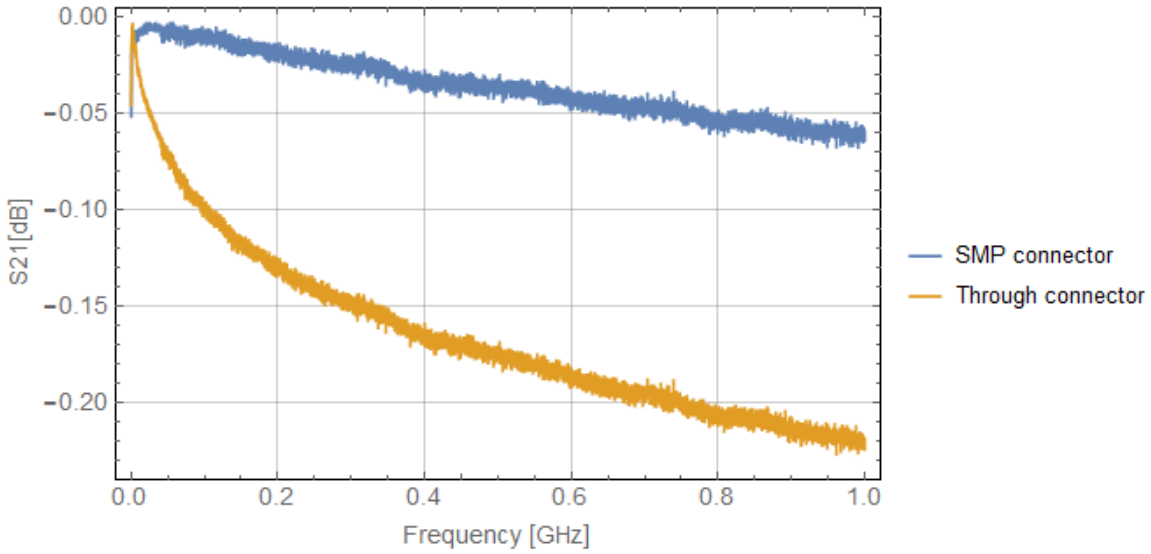

Figure 6: Transmission of the two SMP connectors soldered together placed in the through line of the VNA (blue) compared to a standard through connector (orange)

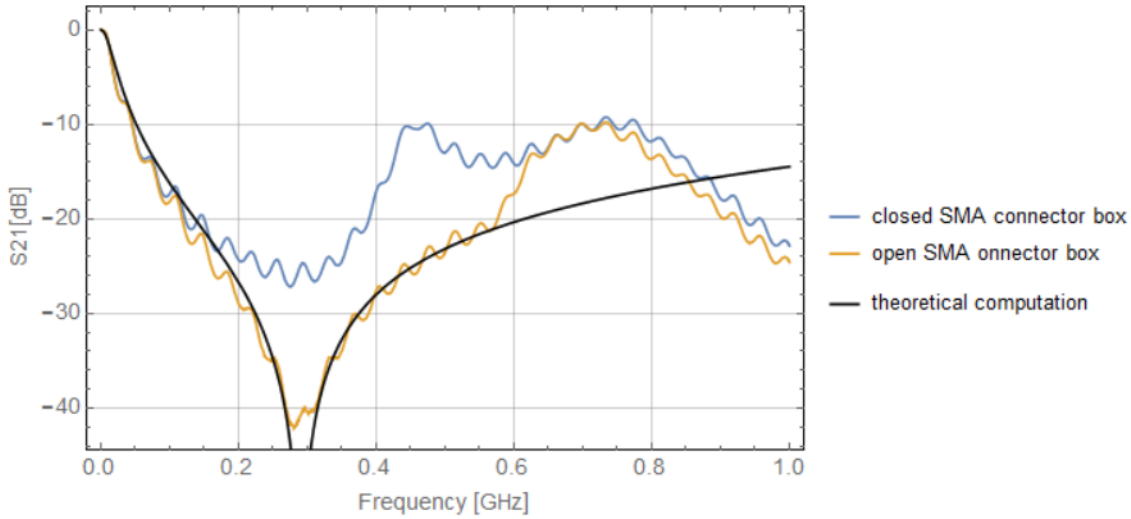

Figure 7: Scattering parameter S21 of coil 2 with N=15 windings placed inside a SMA connector box which is once open (blue) and closed (orange), theoretical prediction (black)

theoretical prediction, we need an experimentally determined value for the inductance of the coil, using a voltage divider formula for the coil on the through line, between points 1 and 2 of Figure 4:

$$Z_{DUT} = 2 \cdot 50\Omega(\frac{1}{S_{21}} - 1) \tag{3}$$

So that one gets this exact relationship valid for any impedance of the DUT one has to perform a second order analysis of the equivalent circuit of a two port VNA acting as a voltage divider [4] shown in Figure 4. In Figure 8 one can see a nice correspondance between the experimental and theoretical values computed from the transmission line model using equation 2.

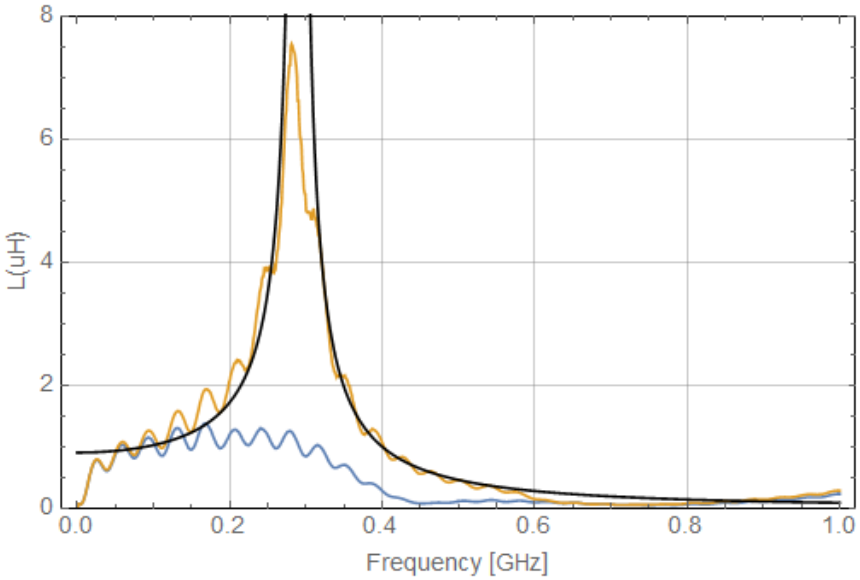

Figure 8: Inductance of coil 2 with 15 windings inside a SMA connector box closed (blue) and open (orange) computed from the measured scattering parameters, compared to the the plot of the inductance around the SRF computed from the transmission line theroy (black)

As we want to test our device in a situation as close to the final setup as possible, we will measure from now on a setup where we put the soldered SMP connectors between the points 1 and 2 of Figure 4 which simulates the RF line. The inductor acts as the DUT and is joined to a resistance between points 3 and 4 and then to the ground. This setting is used to depict the DC line of the final setup, with the resistance of 1 kΩ simulating

several low pass filters on that line. Afterwards the resistance is changed to 50 Ω in order to improve the impedance matching. In fact we want a very smooth transmission, so even if in principle the SRF is a nice feature in the sense that it prohibits any current to pass through the inductor and isolates it completely, it creates an inhomogeneosity in the transmission as the effective impedance of the inductor decreases again beyond the SRF. This leads to

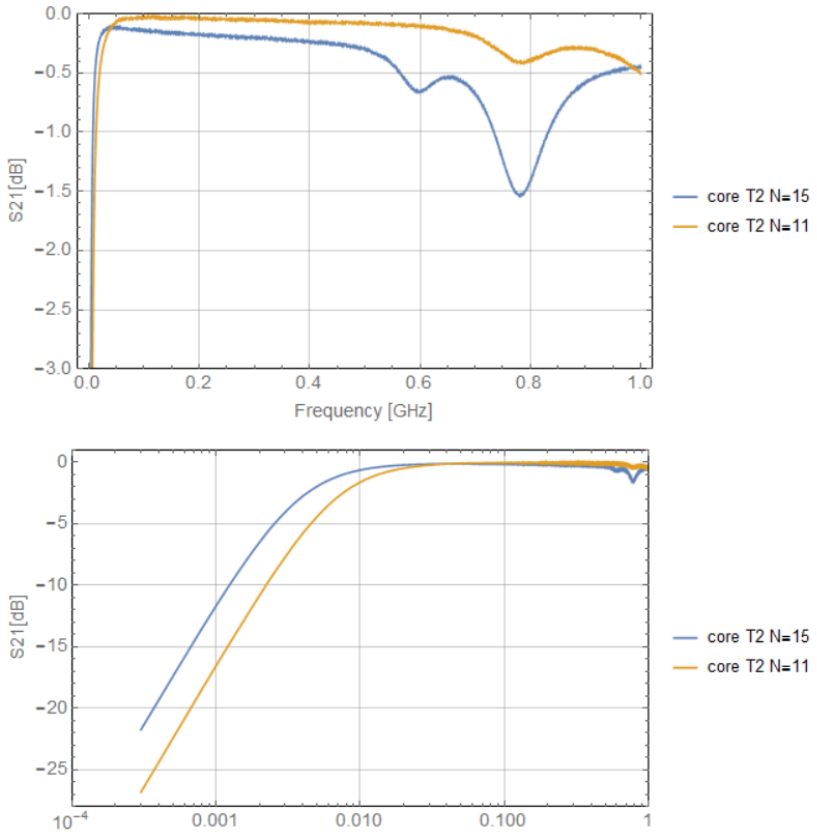

Figure 9: Linear and logarithmic plot of scattering parameter S21 of grounded coil material 2 with number of windings N=15 (blue) and N=11 (orange)

the conclusion that it is desirable to move the SRF beyond the frequency range we're interested in. The expression for the self-resonance frequency for a LC circuit suggests that we use a lower inductance, and try to minimize the parasitic capacitance, still keeping in mind not to lower the inductance too much to keep a reasonable cutoff frequency. That's why we reduce the

number of windings from N=15 to N=11 and compare the measurements in Figure 9 where the coil has been directly grounded. The approvements in the transmission are clearly visible in the linear plot as well as a small degradation of the cutoff frequency which one can see in the logarithmic plot. We use the standard definition for the cutoff frequency consiting of the increase of the tranmission to -3dB, which gives us a frequency around 3.7 MHz for N=15 and 6.8 MHz for N=11. This provides the motivation to proceed with a coil with higher permeability but fewer windings. To check

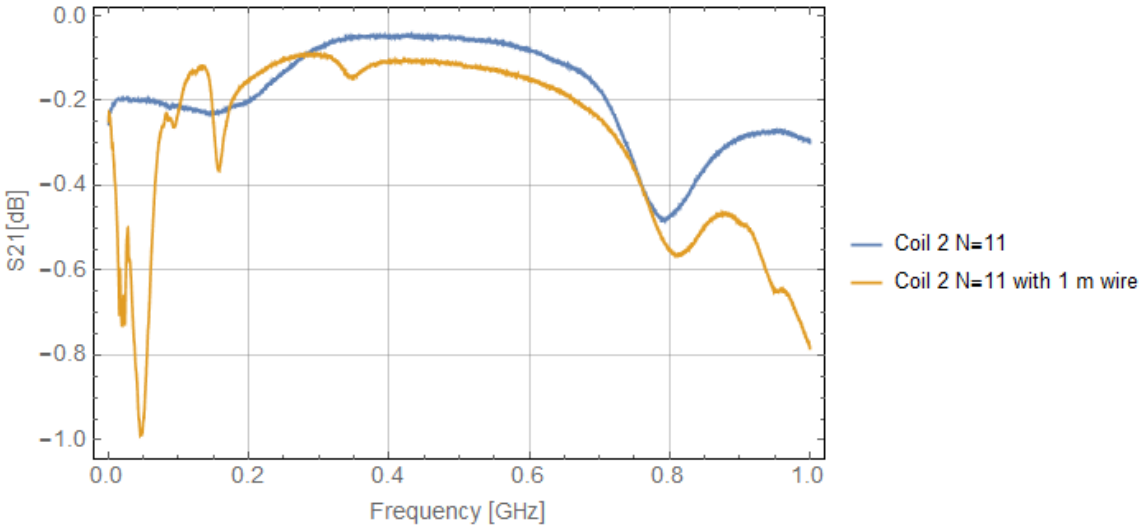

Figure 10: Scattering parameter S21 of grounded coil material 2 with number of windings N=11 (blue) and connected to a 1m wire in between the coil and 1 kΩ resistance to the ground (orange)

for the case where the distance between the coil and the resistance we insert a simple wire of 1m length between the coil, between point 3 of Figure 4 and the 1kΩ resistance to ground at point 4. The scattering parameter S21 shown in Figure 10 illustrates the perturbations most likely caused by standing waves on the wire in the transmission, especially for low frequencies. For higher frequencies, above the SRF the main feature around 0.8 GHz seems unchanged, which then must be caused by the wound wire around the coil together with the coil itself which sem to oppress the appearance of the standing waves. One also notices that the increase in Figure 10, around a frequency of 0.3 GHz corresponds to what one would expect to be the self-resonance frequency of the inductor shown in Figure 8.

As the impedance of the DUT at low frequencies is determined by the

additional resistance, one can verify the sensitivity of the measurement by using the value of the scattering parameter at 300 kHz, S21 = - 0.22 dB together with the general formula for the impedance of the device under test (DUT) as shown in Figure 4

$$Z_{DUT} = 25\Omega \frac{S_{21}}{1 - S_{21}} \tag{4}$$

we find that Z_{DUT}=999.5 Ω which is very close to the 1kΩ that we would expect.

Temperature stability The measurement results of both materials with 11 windings mounted on a dipstick in liquid N_2 shown in Figure 11 indicate that, especially for low freuqencies there is a more significant difference in comparison to the measurements at room temperature for material 3 than for material 2. For all the measurements the calibration of the dipstick has been done at room temperature. The logarithmic plot in Figure 11 also illustrates the cutoff frequencies. In this case where the coil is connected to a 50 Ω resistance before the ground, we define the cutoff as the frequency at which the transmission is -1.25 dB because we define it as half of what we expect for the DC case (-3.5 dB) from equation 4 with Z_{DUT}=50Ω. For core 2 this leads to a frequency which increases from 22 MHz to 31 MHz when it is cooled down in liquid nitrogen. For core 3 with 11 windings the decrease in temperature changes the frequency from 8 MHz to 16 MHz and for 8 windings it is 17 MHz at room temperature. All together we can see that the number of windings of coil 3 can be reduced to 8 in order to improve the tansmission without changing the inductance too much.

In Figure 15 one can see the scattering parameters of coil 3 with the number of windings reduced to 8 at room temperature, together with the same setup mounted on a dipstick in liquid helium. The decrease in temperature increases the cutoff frequency for core T2 from 22 MHz at room temperature to 27 MHz at 4 K and for core T3 from 15MHz to 40 MHz. This figure also clearly shows that the temperature stability of the core T2 is far better than that of the core T3.

Additionally we notice the tendency of the S21 scattering parameter, especially for Coil 3 to increase progressiveley with higher frequencies above 0 dB. It seems sensible that this effect is due to an overcompensation of the improved conductivity at low temperatures of the dipstick which we calibrated at room temperature. This motivates the measurement of a dipstick with a through connector only in liquid Helium which, shown in Figure 13 confirms this assumption. From now on the scattering parameters at low

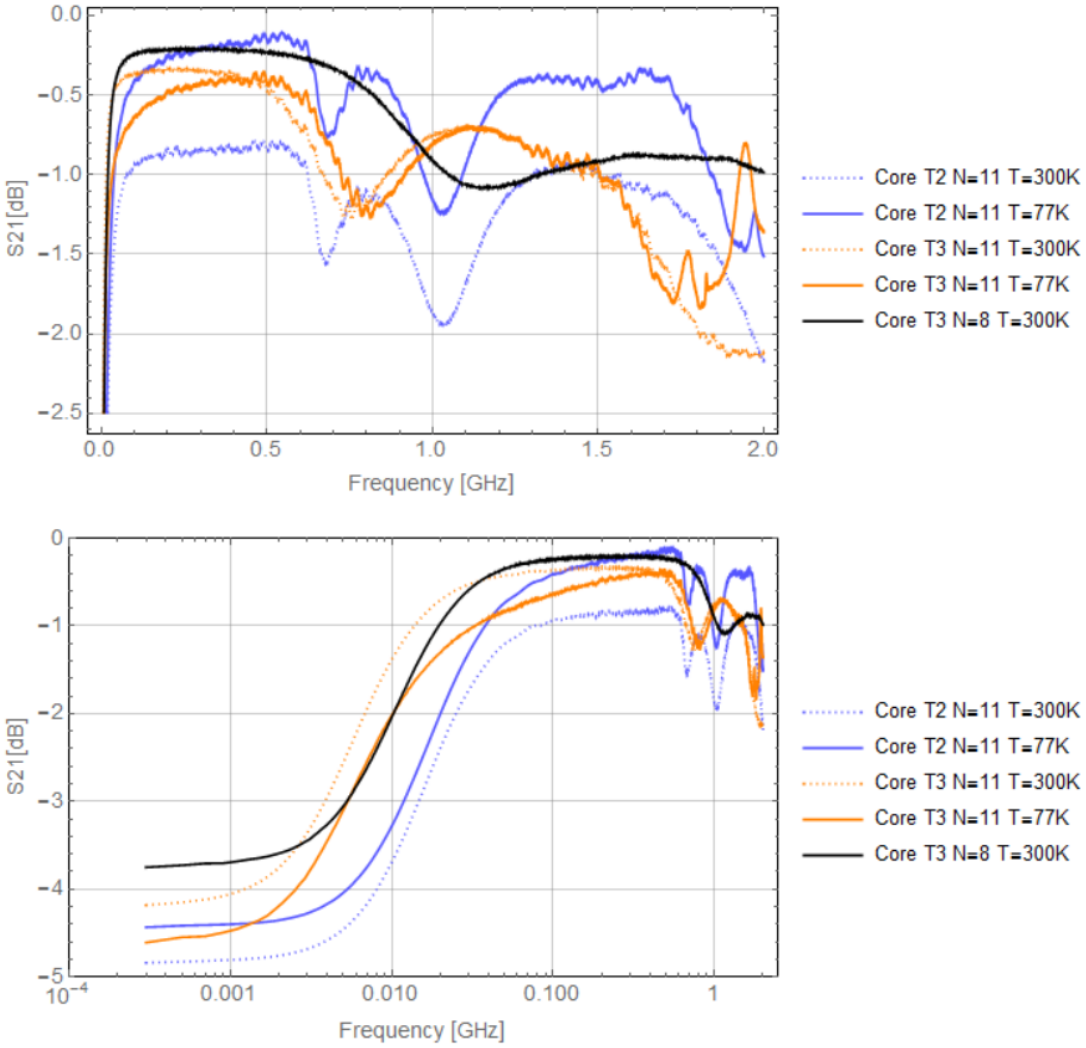

Figure 11: Linear and logarithmic plot of scattering parameter S21 of the coils grounded to 50 Ω resistance with number of windings N=11 material 2 (blue) in liquid nitrogen and at room temperature(dashed), material 3 N=11 (orange) in liquid nitrogen and at room temperature (dashed) and material 3 N=8 at room temperature (black)

temperatures will be rescaled accordingly and the difference between the original and the rescaled data is illustrated in Figure 14 which shows a small but distinguishable improvement.

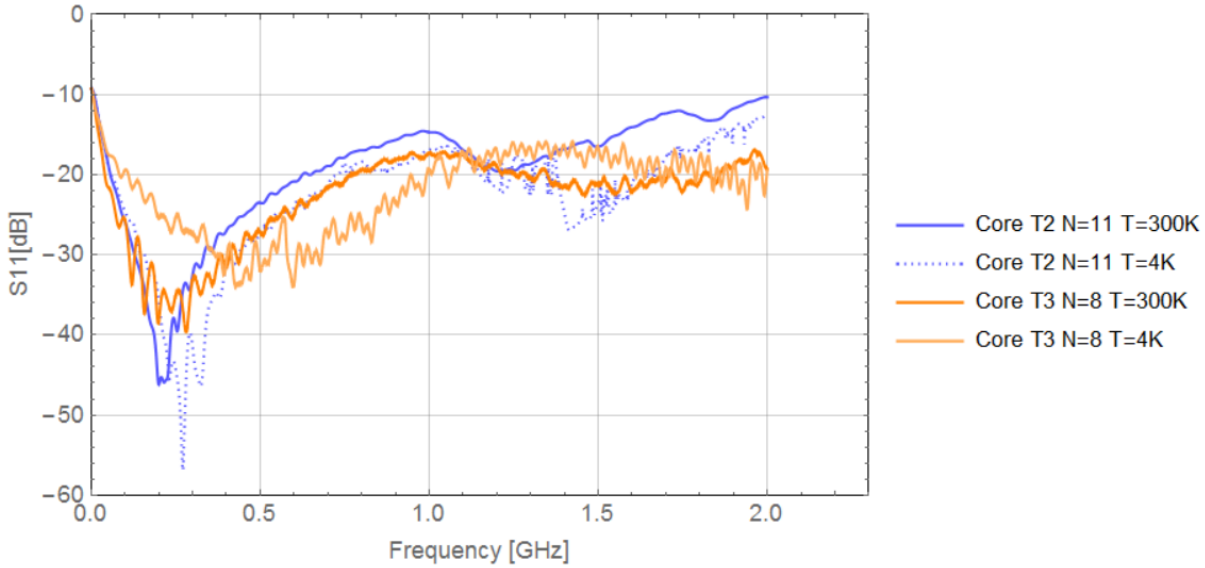

Figure 12: Scattering parameter S11 of Core T2 (blue) with number of windings N=11, and Core T3 (orange) with N=8 both grounded to a 50 Ω resistance at room temperature and in liquid Helium (dahed blue, lighter orange)

Assuming that the temperature dependent variable is in fact the relative permeability of the iron powder core, the change in inductance of the toroid can be determined from the displacement of the SRF from room temperature to 4 K visible in the S11 plot in Figure 12 using $f_r = 1/2\pi\sqrt{LC}$, and we find $L_{Coil3,300K}$=0.77μH and $L_{Coil3,4K}$=0.26μH. The inductance can also be estimated from the S21 parameter using the expression 4 with $Z_{DUT} = 50\Omega + iwL$. At a decline of -1.5dB from the maximal transmission one finds the inductances $L_{Coil3,300K}$=0.84μH and $L_{Coil3,4K}$=0.31μH which means that both methods provide similar results. If we repeat both this calculations we find from the displacmenet of the SRF that $L_{Coil2,300K}$=0.629μH and $L_{Coil2,4K}$=0.483μH which is a much smaller change than it was for Coil 3. If we use the method of the attenuation of the S21 parameter we find similarily $L_{Coil2,300K}$=0.55μH and $L_{Coil2,4K}$=0.48μH which again is consistent with the theoretical prediction for low frequencies, and with the result of the SRF displacement.

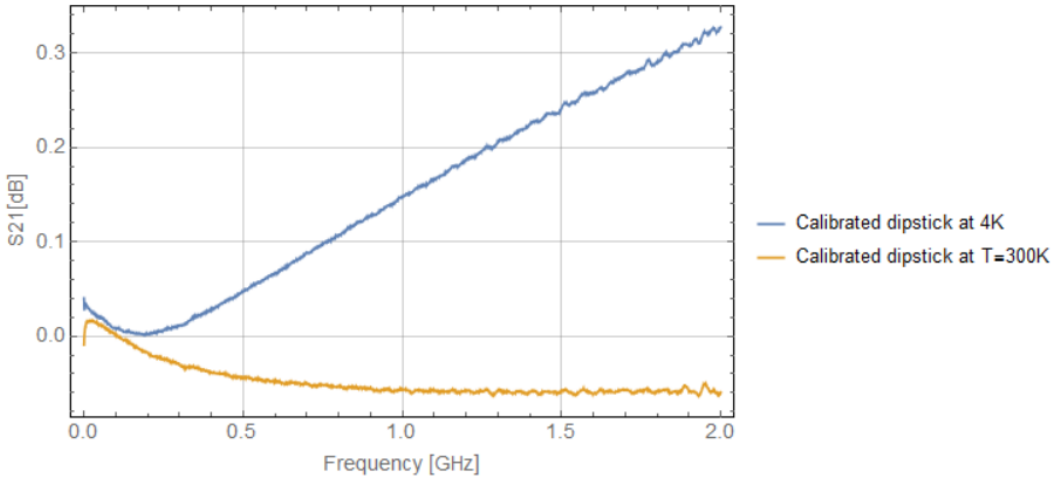

Figure 13: Scattering parameter S21 of the dipstick calibrated at room temperature, measured with a through connector at T=4K (blue) and at room temperature (orange)

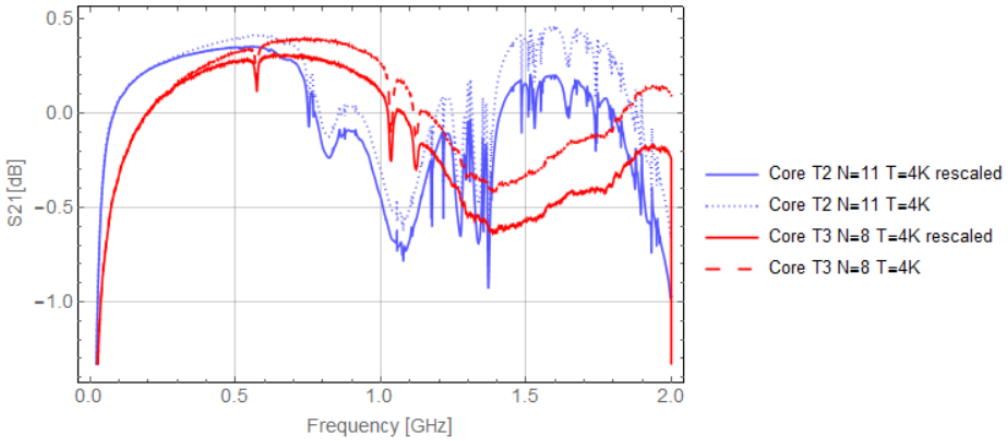

Figure 14: Scattering parameter S21 of Core T2 with number of windings N=11 (blue) and Core T3 with N=8 (red), both grounded to a 50 Ω resistance in liquid Helium rescaled and raw data (dashed)

4.2 SMD inductors

Measuring th scattering parameters of the SMD inductors in the same way as for the coils, soldering them to a 50 Ω resistance and to the SMP connectors,

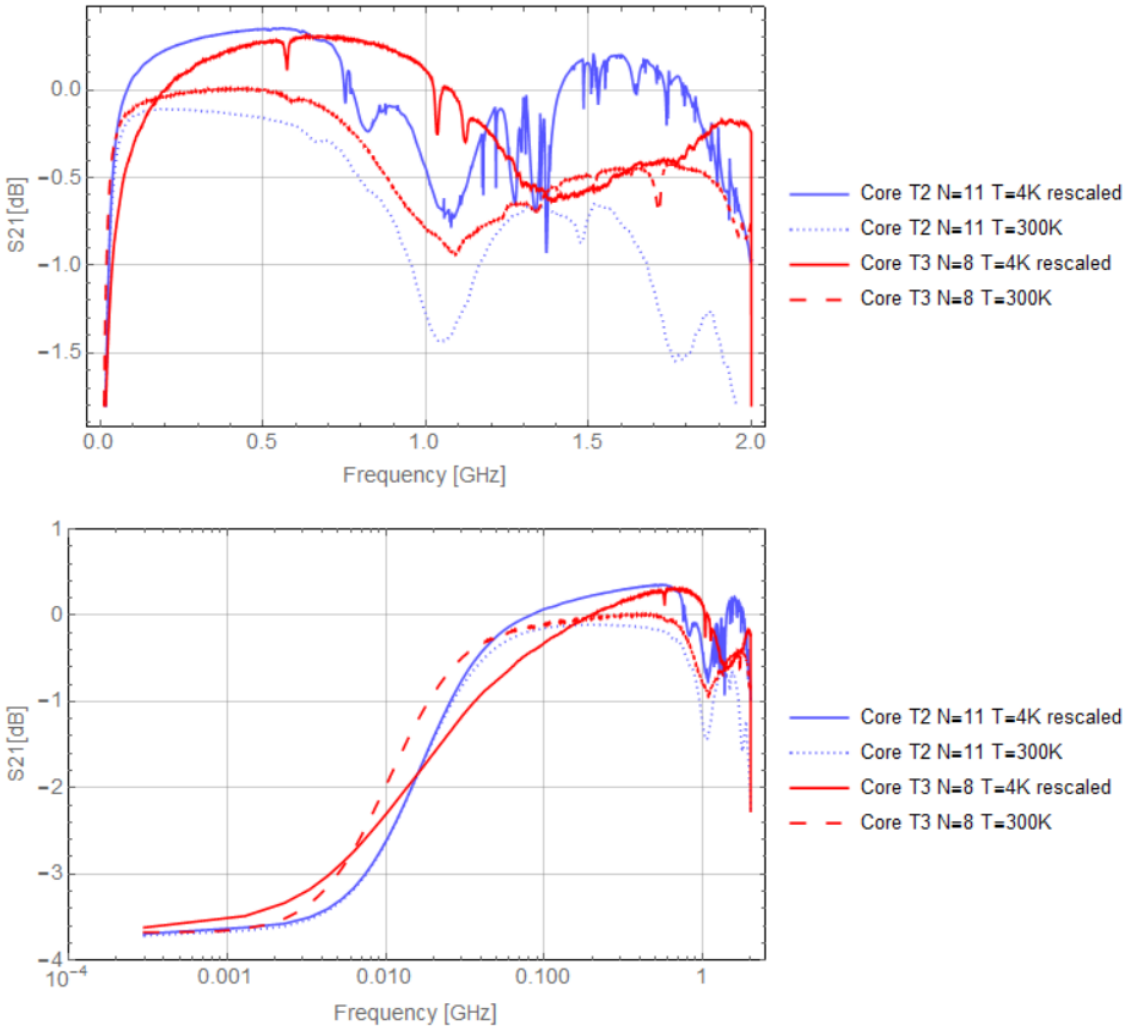

Figure 15: Linear and logarithmic plot of scattering parameter S21 of Core T2 with number of windings N=11 (blue) and Core T3 with N=8 (red), both grounded to a 50 Ω resistance at room temperature (dashed) and in liquid Helium rescaled

fixing the bias choke on a dipstick, the measurement is taken once at room temperature and once plunged into a tank filled with liquid Helium. The results, shown in Figure 16 illustrate that inductor 300-41-940 delivers the best performance, meaning that it has a quite flat transmission and an acceptable cutoff frequency, changing though from 28MHz at room temperature to

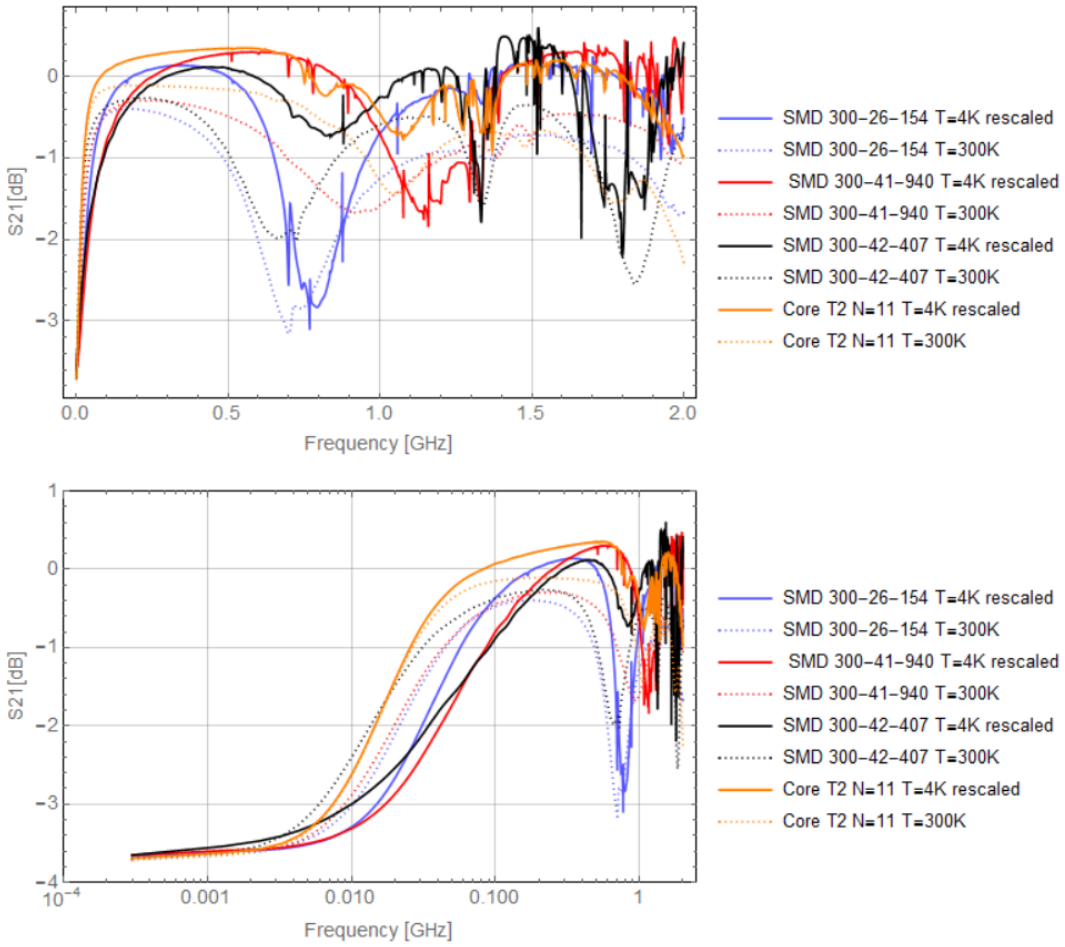

Figure 16: Linear and logarithmic plot of scattering parameter S21 of the SMD inductors 300-26-154 (blue), 300-41-940 (red) and 300-42-407 (black) and the toroidal coil material2 N=11(orange) grounded to a 50 Ω resistance at room temperature (dashed) and in liquid Helium rescaled

87MHz at 4K. For all three SMD inductors however the transmission changes significantly with the cooling, exhibiting a poor temperature stability, which makes them unusable for our purposes. If we compare their performance to the toroidal inductor with core material 2 also plotted in Figure 16 we notice that not only the temperature stability, but also the cutoff frequency which one can clearly see on the logarithmic plot is worse for the SMD inductors. All together we can conclude that the coil is the better choice .

5 Conclusion

Comparing all the measurements for both the coils and the SMD inductors together we can conclude that overall the toroidal inductors have a better temperature stability than the SMD inductors. Also it is advantageous to use as few windings as the cutoff frequency allows in order to minimize the parasitic capictances which tamper the low pass filter performance of the coil. Even if this criterium would favour us to choose T-37 iron powder toroids with material 3, the crucial argument remains the temperature stability which makes the T-37 iron powder toroids with material 2 preferable.

6 Bibliography

References

[1] Bias Tee 2.0 Daniel Staudigel

[2] The Self-Capacitance of Toroidal Inductors Âĺ D W Knight 2008, 2015, 2016

[3] The self-resonance and self-capacitance of solenoid coils: applicable theory, models and calculation methods. By David W Knight

[4] Agilent Ultra-Low Impedance Measurements Using 2-Port Measurements Application Note

[5] The self-capacitance of single layer toroidal inductors with ferrite cores Âĺ Alan Payne 2015

[6] www.distrelec.ch

[7] Eavluate Your 3D Inductor Design with COMSOL Multiphysics, Comsol Blog, Scott Smith, 19 April 2016